Spin-Orbit Coupling Induced Spin-Transfer Torque and Current Polarization in Topological-Insulator/Ferromagnet Vertical Heterostructures

Farzad Mahfouzi,[1] Naoto Nagaosa,[2,3] and Branislav K. Nikolić[1,2,*]

[1]*Department of Physics and Astronomy, University of Delaware, Newark, Delaware 19716-2570, USA*
[2]*Cross-Correlated Materials Research Group (CMRG) and Correlated Electron Research Group (CERG), RIKEN-ASI, Wako, Saitama 351-0198, Japan*
[3]*Department of Applied Physics, University of Tokyo, Tokyo 113-8656, Japan*

(Received 9 March 2012; published 17 October 2012)

We predict an unconventional spin-transfer torque (STT) acting on the magnetization of a free ferromagnetic (F) layer within N/TI/F vertical heterostructures, which originates from strong spin-orbit coupling on the surface of a three-dimensional topological insulator (TI), as well as from charge current becoming spin polarized in the direction of transport as it flows perpendicularly from the normal metal (N) across the bulk of the TI layer. The STT vector has both in-plane and perpendicular components that are comparable in magnitude to conventional torque in F′/I/F (where I stands for insulator) magnetic tunnel junctions, while not requiring additional spin-polarizing F′ layer with fixed magnetization, which makes it advantageous for spintronics applications. Our principal formal result is a derivation of the nonequilibrium Green function-based formula and the corresponding gauge-invariant nonequilibrium density matrix, which makes it possible to analyze the components of the STT vector in the presence of arbitrary strong spin-orbit coupling either in the bulk or at the interface of the free F layer.

DOI: 10.1103/PhysRevLett.109.166602 PACS numbers: 72.25.Mk, 72.10.Bg, 75.70.Tj, 85.75.−d

The spin-transfer torque (STT) is a phenomenon in which a spin current of large enough density injected into a ferromagnetic (F) layer either switches its magnetization from one static configuration to another or generates a dynamical situation with steady-state precessing magnetization [1]. The origin of the STT is the absorption of the itinerant flow of angular momentum components normal to the magnetization direction. It represents one of the central phenomena of the second-generation spintronics, focused on the manipulation of coherent spin states, since the reduction of current densities (currently of the order 10^6–10^8 A/cm^2) required for STT-based magnetization switching is expected to bring about commercially viable magnetic random access memory (MRAM) [2]. The rich nonequilibrium physics [3] arising in the interplay of spin currents carried by fast conduction electrons and collective magnetization dynamics, viewed as the slow classical degree of freedom, is of great fundamental interest.

Very recent experiments [4,5] and theoretical studies [6] have sought the STT in nontraditional setups which do not involve the usual two (spin-polarizing and free) F layers with noncollinear magnetizations [3], but rely instead on the spin-orbit coupling (SOC) effects in structures lacking inversion symmetry. Such *SO torques* [7] have been detected [4] in Pt/Co/AlO$_x$ lateral devices where current flows in the plane of the Co layer. Concurrently, the recent discovery [8] of three-dimensional (3D) topological insulators (TIs), which possess a usual band gap in the bulk while hosting metallic surfaces whose massless Dirac electrons have spins locked with their momenta due to the strong Rashba-type SOC, has led to theoretical proposals to employ these exotic states of matter for spintronics [9] and the STT in particular [10]. For example, the magnetization of a ferromagnetic film with perpendicular anisotropy deposited on the TI surface could be switched by the interfacial quantum Hall current [10]. However, very little is known about the STT in setups where spin transport is perpendicular to interfaces with strong SOC [11–13], as exemplified by the vertical TI-based heterostructure in Fig. 1. Such heterostructures could exploit strong interfacial SOC without requiring [13,14] a perfectly insulating bulk whose unintentional doping in the present experiments obscures [15] the topological properties anticipated for lateral transport along the TI surface.

In this Letter, we predict that the heterostructure in Fig. 1 will exhibit an unconventional STT, driven both by the surface SOC and spin-polarizing effect of the bulk of the TI

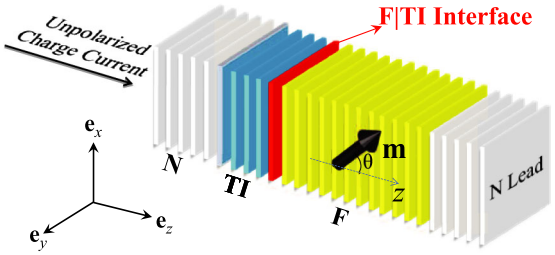

FIG. 1 (color online). Schematic view of the topological insulator-based vertical heterostructure operated by spin-transfer torque. The junction contains a single F layer of finite thickness with free magnetization **m**, and the N leads are semi-infinite. We assume that each layer is composed of atomic monolayers (modeled on an infinite square tight-binding lattice).

slab on the current flowing perpendicularly through it. Its unusual features depicted in Fig. 2(a) could also open new avenues in the design of STT-MRAM [16] and STT-oscillators [17]. For example, in conventional collinearly magnetized STT-MRAM devices [2], the initial current-induced STT is zero so that one has to rely on thermal fluctuations or small misalignments of the layer magnetizations to initiate the switching. Such undesirable long mean switching times and broad switching time distributions can be avoided by adding a TI capping layer onto the standard F/I/F′ (where I stands for insulator) magnetic tunnel junction (MTJ), to form a TI/F/I/F′ vertical heterostructure (see Sec. II in the Supplemental Material [18]), where the TI layer will initiate fast switching of the F layer magnetization in accord with Fig. 2(a).

Our second principal result is a nonequilibrium Green function (NEGF)-based formula, and the related gauge-invariant nonequilibrium density matrix (see Sec. III in the Supplemental Material [18]), which makes it possible to analyze the torque components in the presence of arbitrary spin-current nonconserving interactions within the device. Unlike the recently developed approaches [19,20] to the STT in the presence of SOC for the linear-response regime, ours can handle torque driven by finite bias voltage (required to reach sufficient current density in MTJs [3]), and

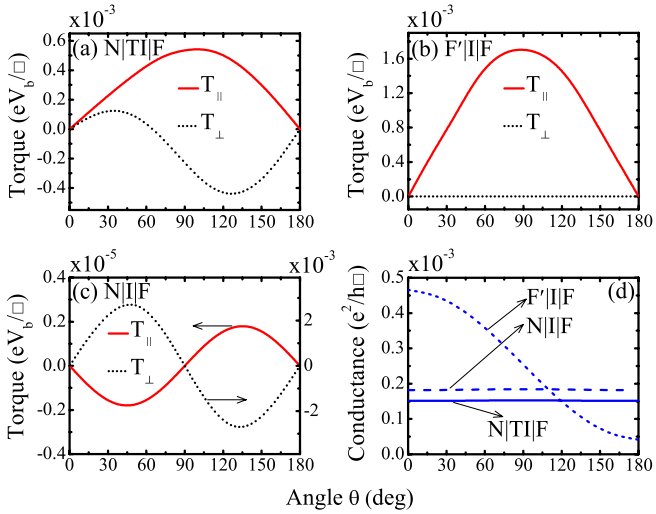

FIG. 2 (color online). (a) The angular dependence of torque components, $\mathbf{T}_{\parallel} = \tau_{\parallel}\mathbf{m} \times (\mathbf{m} \times \mathbf{e}_z)$ and $\mathbf{T}_{\perp} = \tau_{\perp}\mathbf{m} \times \mathbf{e}_z$, acting on the free magnetization $\mathbf{m}$ within N/TI/F heterostructure in Fig. 1. (b) The torque components, $\mathbf{T}_{\parallel} = \tau_{\parallel}\mathbf{m} \times (\mathbf{m} \times \mathbf{m}')$ and $\mathbf{T}_{\perp} = \tau_{\perp}\mathbf{m} \times \mathbf{m}'$, acting on the free-layer magnetization $\mathbf{m} = (\sin\theta\cos\phi, \sin\theta\sin\phi, \cos\theta)$ in conventional F′/I/F symmetric MTJ where magnetization of the reference layer F′ is fixed at $\mathbf{m}' = \mathbf{e}_z$. (c) The torque components in N/I/F junction, defined in the same fashion as in panel (a), with the Rashba SOC of strength $\alpha_R/2a = 0.1$ eV located on the last monolayer of F which is in contact with I barrier. (d) The angular dependence of conductances for N/TI/F, F′/I/F and N/I/F junctions. The bias voltage V_b in all panels is sufficiently small to ensure the linear-response regime.

it can also be easily combined with density functional theory (DFT) through the NEGF-DFT formalism [21,22].

For conventional F′/I/F MTJs, where the reference F′ layer with fixed magnetization $\mathbf{m}'$ plays the role of an external spin polarizer, it is customary to analyze the in-plane (originally considered by Slonczewski [23]) and perpendicular (also called *fieldlike torque* [1]) components of the STT vector [3], $\mathbf{T} = \mathbf{T}_{\parallel} + \mathbf{T}_{\perp}$. The in-plane torque $\mathbf{T}_{\parallel} = \tau_{\parallel}\mathbf{m} \times (\mathbf{m} \times \mathbf{m}')$ is purely a nonequilibrium component and competes with the damping. The perpendicular torque $\mathbf{T}_{\perp} = \tau_{\perp}\mathbf{m} \times \mathbf{m}'$ arises from spin reorientation at the interfaces and possesses both equilibrium (i.e., interlayer exchange coupling) and nonequilibrium contributions which act like an effective magnetic field on the magnetization $\mathbf{m}$ of the free F layer. While the $\mathbf{T}_{\perp}$ component is vanishingly small in metallic spin valves [24,25], it can be substantial [3] in MTJs due to the momentum filtering imposed by the tunnel barrier [26,27].

To understand the origin of the torque components in Fig. 2(a), we first elucidate the effect of the TI slab on the unpolarized charge current injected from the left normal metal (N) lead by computing the spin density matrix $\hat{\rho}^{\rm out}_{\rm spin} = \frac{1}{2}(1 + \mathbf{P}^{\rm out} \cdot \hat{\boldsymbol{\sigma}})$ for an ensemble of outgoing spin in the right N lead of the N/TI/N junction. The expression for $\hat{\rho}^{\rm out}_{\rm spin}$, or equivalent spin-polarization vector $\mathbf{P}^{\rm out}$, was derived as Eq. (10) in Ref. [28] in terms of the transmission matrix of the device. Its evaluation for the N/TI/N junction is plotted in Fig. 3, which shows how the TI slab polarizes the incoming current in the direction of transport with $\mathbf{P}^{\rm out} = (0, 0, \simeq 0.5)$. The polarizing effect of the TI slab comes from the effective momentum-dependent magnetic field along the z axis [encoded by the $\mathbf{\Gamma}_3$ term in the TI Hamiltonian in Eq. (3) discussed below]. This requires sufficient thickness of the TI slab, as well as that the Fermi energy of the device E_F be within the bulk gap of the TI. The spin polarization of the charge current induced by its flow through a finite-size region with SOC has been discussed previously for low-dimensional systems (such as the two-dimensional electron gas with the Rashba SOC

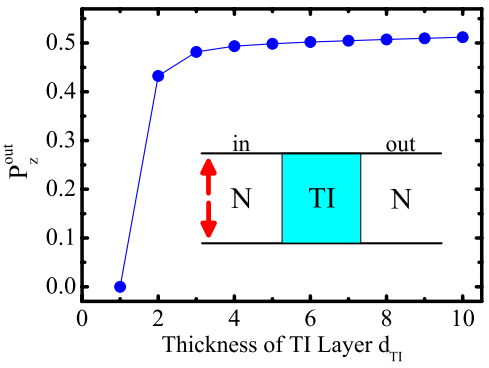

FIG. 3 (color online). The spin-polarization vector $\mathbf{P}^{\rm out} = (0, 0, P^{\rm out}_z)$ of current [28] in the right N lead of N/TI/N junction as a function of the thickness $d_{\rm TI}$ of the 3D TI layer after unpolarized charge current is injected from the left N lead.

[29]). Due to constraints imposed by the time-reversal invariance, such SOC-induced polarization cannot [29] be detected via current or voltage measurement on standard two-terminal ferromagnetic circuits, as exemplified by Fig. 2(d) where the conductance of the N/TI/F junction is the same for $\mathbf{m} \parallel \mathbf{e}_z$ and $\mathbf{m} \nparallel \mathbf{e}_z$ configurations.

Following this analysis, the meaning of the torque components in Fig. 2(a) for the N/TI/F junction is explained by

$$\mathbf{T} = \mathbf{T}_{\parallel} + \mathbf{T}_{\perp} = \tau_{\parallel} \mathbf{m} \times (\mathbf{m} \times \mathbf{e}_z) + \tau_{\perp} \mathbf{m} \times \mathbf{e}_z. \quad (1)$$

The nonzero values of both $\mathbf{T}_{\parallel}$ and $\mathbf{T}_{\perp}$ in the N/TI/F junction make this SOC-driven STT quite different from recently explored *SO torques* [4,6,7] which lack an antidamping (i.e., equivalent to our $\mathbf{T}_{\parallel}$) component and, therefore, cannot induce a precession of the magnetization in the single F layer. We note that the same definition of the torque components is applicable [12] also to N/I/F vertical heterostructures with strong Rashba SOC, $\alpha_R(\hat{\boldsymbol{\sigma}} \times \mathbf{k}_{\parallel}) \cdot \mathbf{e}_z$, at the I/F interface [4,7] even though the current does not become polarized along $\mathbf{e}_z$ there. The torque components for the N/I/F junction plotted in Fig. 2(c) are driven purely by the surface Rashba SOC, which is the second order effect $\propto \alpha_R^2$ characterized by torque asymmetry [12] around the stable magnetic state $\theta = 90°$. On the other hand, $\mathbf{T}_{\parallel}$ and $\mathbf{T}_{\perp}$ in Fig. 2(a) are nonzero at $\theta = 90°$ in N/TI/F junctions due to the summation (see Sec. I in the Supplemental Material [18]) of an asymmetric contribution driven by the strong SOC on the surface of the TI layer and a symmetric one [akin to conventional torque in MTJs shown in Fig. 2(b)] driven by the spin polarization [Fig. 3] of current flowing through the bulk of the TI layer.

Figures 2(a) and 2(b) show that linear-response $\mathbf{T}_{\parallel}$ in N/TI/F junctions is comparable to the one in symmetric F′/I/F MTJs tuned (via the on-site potential in the I layer) to have similar conductance, which points to unforeseen [9] spintronics applications of TIs. The angular dependence of the conductances for the N/TI/F, N/I/F, and F′/I/F junctions are compared in Fig. 2(d).

We now turn to the details of our formalism. The junction in Fig. 1 is modeled on a cubic lattice, with lattice constant a and unit area $a^2 \equiv \square$, where the monolayers of the different materials (N, F, TI) are infinite in the transverse xy direction. The TI layer has thickness $d_{\mathrm{TI}} = 5$ monolayers and the free F layer has thickness $d_F = 70$ monolayers. The F and N layers are described by a tight-binding Hamiltonian with a single s orbital per site

$$\hat{H}_F = \sum_{n,\sigma\sigma',\mathbf{k}_{\parallel}} \hat{c}^{\dagger}_{n\sigma,\mathbf{k}_{\parallel}} \left(\varepsilon_{n,\mathbf{k}_{\parallel}} \delta_{\sigma\sigma'} - \frac{\Delta_n}{2} \mathbf{m} \cdot [\hat{\boldsymbol{\sigma}}]_{\sigma\sigma'} \right) \hat{c}_{n\sigma',\mathbf{k}_{\parallel}} - \gamma \sum_{n,\sigma,\mathbf{k}_{\parallel}} (\hat{c}^{\dagger}_{n\sigma,\mathbf{k}_{\parallel}} \hat{c}_{n+1,\sigma,\mathbf{k}_{\parallel}} + \mathrm{H.c.}). \quad (2)$$

The operators $\hat{c}^{\dagger}_{\mathbf{n}\sigma}$ ($\hat{c}_{\mathbf{n}\sigma}$) create (annihilate) an electron with spin σ on a monolayer n with transverse momentum $\mathbf{k}_{\parallel}$ within the monolayer. The in-monolayer kinetic energy $\varepsilon_{n,\mathbf{k}_{\parallel}} = -2\gamma(\cos k_x a + \cos k_y a)$ is equivalent to an increase in the on-site energy, and the nearest neighbor hopping is $\gamma = 1.0$ eV. The coupling of itinerant electrons to collective magnetization dynamics is described through the material-dependent exchange potential $\Delta_n = 1.0$ eV ($\Delta_n \equiv 0$ within semi-infinite ideal N leads), where $\hat{\boldsymbol{\sigma}} = (\hat{\sigma}_x, \hat{\sigma}_y, \hat{\sigma}_z)$ is the vector of the Pauli matrices and $[\hat{\sigma}_{\alpha}]_{\sigma\sigma'}$ denotes the Pauli matrix elements.

The minimal model for the slab of a 3D TI, such as Bi_2Se_3, is the effective tight-binding Hamiltonian with four orbitals per site [30]:

$$\hat{H}_{\mathrm{TI}} = \sum_{n,\mathbf{k}_{\parallel}} \left\{ \mathbf{c}^{\dagger}_{n,\mathbf{k}_{\parallel}} \left(\frac{B}{a^2} \boldsymbol{\Gamma}_0 - i \frac{A}{2a} \boldsymbol{\Gamma}_3 \right) \mathbf{c}_{n+1,\mathbf{k}_{\parallel}} + \mathrm{H.c.} + \mathbf{c}^{\dagger}_{n,\mathbf{k}_{\parallel}} \left[C\mathbf{1} + d(\mathbf{k}_{\parallel}) \boldsymbol{\Gamma}_0 + \frac{A}{a} (\boldsymbol{\Gamma}_1 \sin k_x a + \boldsymbol{\Gamma}_2 \sin k_y a) \right] \mathbf{c}_{n,\mathbf{k}_{\parallel}} \right\}. \quad (3)$$

It yields the correct gap size in the bulk and surface dispersion while reducing to the continuum $\mathbf{k} \cdot \mathbf{p}$ Hamiltonian in the small k limit. Here $\hat{\mathbf{c}} = (\hat{c}_{+\uparrow}, \hat{c}_{+\downarrow}, \hat{c}_{-\uparrow}, \hat{c}_{-\downarrow})^T$ annihilates an electron in different orbitals, $d(\mathbf{k})_{\parallel} = M - 2B/a^2 + 2B(\cos k_x a + \cos k_y a - 2)/a^2$, $\boldsymbol{\Gamma}_i$ ($i = 0, 1, 2, 3$) are 4×4 Dirac matrices, and $\mathbf{1}$ is the unit matrix of the same size. The numerical values of the parameters are chosen as $M = 0.3$ eV, $A = 0.5a$ eV, and $B = 0.25a^2$ eV. The Fermi energy of the whole device is set at $E_F = 3.1$ eV, and the bottom of the band of the TI layer is shifted by $C = 3.0$ eV.

The hopping $\gamma_c = 0.25$ eV between F or N monolayers and the TI monolayer is chosen to ensure that the Dirac cone on the surface of the TI is not distorted [13,14] by the penetration of evanescent modes from these neighboring metallic layers. The weak F to TI coupling can be achieved by growing an ultrathin layer of a conventional band insulator, such as In_2Se_3 with a large bandgap and good chemical and structural compatibility with Bi_2Se_3 where sharp heterointerfaces have already been demonstrated by molecular-beam epitaxy growth [31]. We assume that such a layer is present and suppresses the magnetic proximity effect so that $\Delta_n = 0$ on the TI monolayer (denoted as the F/TI interface in Fig. 1) that is closest to the F layer.

The early phenomenological modeling [23] of the STT in noncollinear ferromagnetic multilayers was succeeded by more microscopic theories [21,24–27,32], often in combination with first-principles input about real materials [21,24,25,32]. These theories have been focused on devices without SOC where the STT is directly connected to the divergence of the spin current as a consequence of the conservation of total spin. Thus, the STT vector can be obtained simply from the local spin current at the N/F or I/F interface within F′/N/F spin valves or F′/I/F MJTs. Such local spin currents are typically computed using the Landauer-Bütikker scattering approach [25,32] or the NEGF formalism [21,24,27]. However, these

methodologies are inapplicable to junctions with SOC within the free F layer, which has recently ignited a search for efficient algorithms [19–21] that can compute the STT in the presence of spin nonconserving interactions. The SOC can be introduced into the device by either bulk ferromagnets (as in F layers based on ferromagnetic semiconductors [7,19,20]) or due to the Rashba SOC at the I/F interface in devices with structural inversion asymmetry [4,7].

Using the operator $\hat{c}^{\dagger}_{n\sigma}$ ($\hat{c}_{n\sigma}$) which creates (annihilates) an electron with spin σ on a monolayer n, we can introduce the two fundamental objects [33] of the NEGF formalism—the retarded $G^{r,\sigma\sigma'}_{nn'}(t,t') = -i\Theta(t-t')\langle\{\hat{c}_{n\sigma}(t), \hat{c}^{\dagger}_{n'\sigma'}(t')\}\rangle$ and the lesser $G^{<,\sigma\sigma'}_{nn'}(t,t') = i\langle\hat{c}^{\dagger}_{n'\sigma'}(t')\hat{c}_{n\sigma}(t)\rangle$ Green functions (GFs) that describe the density of available quantum states and how electrons occupy those states, respectively. Here $\langle\ldots\rangle$ denotes the nonequilibrium statistical average [33]. In stationary problems, $\hat{G}^r$ and $\hat{G}^<$ depend only on the time difference $t-t'$ or energy E after the Fourier transform.

In the absence of SOC, one can obtain the STT in F′/N/F spin valves or F′/I/F MTJs by computing [27] the vector of the spin current between two neighboring monolayers n and $n+1$ coupled by the hopping parameter γ:

$$\mathbf{I}^{S}_{n,n+1} = \frac{\gamma}{4\pi}\int dE d\mathbf{k}_{\parallel}\,\mathrm{Tr}_{\sigma}[\boldsymbol{\sigma}(\hat{G}^{<}_{n+1,n} - \hat{G}^{<}_{n,n+1})]. \quad (4)$$

The integration over $\mathbf{k}_{\parallel}$ is required because of the assumed translational invariance in the transverse direction. Since, for conserved spin current, the monolayer-resolved [25] STT is given by $\mathbf{T}_n = -\nabla\cdot\mathbf{I}^S = \mathbf{I}^S_{n-1,n} - \mathbf{I}^S_{n,n+1}$, the total torque on the free F layer is, $\mathbf{T} = \sum_{n=0}^{\infty}(\mathbf{I}^S_{n-1,n} - \mathbf{I}^S_{n,n+1}) = \mathbf{I}^S_{-1,0} - \mathbf{I}^S_{\infty,\infty} = \mathbf{I}^S_{-1,0}$ [27], assuming semi-infinite F electrode. Here the subscripts -1 and 0 refer to the last monolayer of the N or I barrier and the first monolayer of the F layer, respectively. In the multilayers with SOC, such as those in Fig. 1, this methodology to get the STT becomes inapplicable since the spin current will not decay (i.e., $\mathbf{I}^S_{\infty,\infty} \neq 0$) if SOC is present in the bulk of the free F layer [20]. Also, the spin current across the interface $\mathbf{I}^S_{-1,0}$ is insufficient to get the STT if strong SOC is present directly at the interface.

To derive a general NEGF-based expression for the expectation value of the current-induced force, we start by assuming that the device Hamiltonian depends on a variable q which corresponds to slow collective classical degrees of freedom. The expectation value of the corresponding canonical force $\hat{Q} = -\partial\hat{H}/\partial q$ is obtained using the density matrix $\hat{\rho} = \frac{1}{2\pi i}\int dE\hat{G}^<(E,q)$:

$$Q = -\frac{1}{2\pi i}\int_{-\infty}^{+\infty} dE\,\mathrm{Tr}\left[\frac{\partial\hat{H}}{\partial q}\hat{G}^<\right] = -\left\langle\frac{\partial\hat{H}}{\partial q}\hat{G}^<\right\rangle, \quad (5)$$

where $\hat{G}^<(E,q)$ is the adiabatic GF obtained for a frozen-in-time variable q. By exchanging the derivative between the Hamiltonian and $\hat{G}^<(E,q)$, $Q = -\partial\langle\hat{H}\hat{G}^<\rangle/\partial q + \langle\hat{H}\partial\hat{G}^</\partial q\rangle$, and by using the standard equations for the retarded and lesser GFs [33], $\hat{G}^r(E) = [E - \hat{H} - \hat{\Sigma}^r]^{-1}$ and $\hat{G}^<(E) = \hat{G}^r(E)\hat{\Sigma}^<(E)\hat{G}^a(E)$, we finally obtain

$$Q = i\left\langle\frac{\partial\hat{G}^r}{\partial q}\hat{\Sigma}^<\hat{G}^a\hat{\Gamma}\right\rangle - \left\langle\hat{\Sigma}^<\frac{\partial\hat{G}^r}{\partial q}\right\rangle, \quad (6)$$

where the advanced GF is given by $\hat{G}^a = [\hat{G}^r]^{\dagger}$. In the elastic transport regime, $\hat{\Gamma}(E) = \sum_p\hat{\Gamma}_p(E - eV_p)$ is the sum of the level broadening operators $\hat{\Gamma}_p(E-eV_p) = i[\hat{\Sigma}^r_p(E-eV_p) - \hat{\Sigma}^a_p(E-eV_p)]$, $\hat{\Sigma}^r_p(E-eV_p)$ are the self-energies due to the coupling to semi-infinite (F or N) ideal leads $p = L, R$, and $\hat{\Sigma}^<(E) = \sum_p if_p(E)\hat{\Gamma}_p(E-eV_p)$ is the lesser self-energy [33]. The junction is biased by the voltage $V_b = V_L - V_R$ and $f_p(E) = f(E-eV_p)$ is the Fermi function of the macroscopic reservoir to which the lead p is assumed to be attached at infinity. We note that Eq. (6) is akin to the mean value of the time-averaged force in nonequilibrium Born-Oppenheimer approaches [34] to current-induced forces exerted by conduction electrons on ions in nanojunctions or mechanical degrees of freedom in nanoelectromechanical systems whose collective modes are slow compared to electronic time scales.

The application of Eq. (6) to get the T_α ($\alpha = x, y, z$) component of the STT vector acting on the magnetization of the free F layer of finite thickness within the N/TI/F junction proceeds by first computing $\hat{G}^r(E)$ for the device described by the Hamiltonian $\hat{H} = \hat{H}_{\mathrm{TI}} + \hat{H}_F$. In the second step, the Hamiltonian of the F layer is modified

$$\hat{H}^q_F = \hat{H}_F + q\sum_{n,\sigma\sigma',\mathbf{k}_{\parallel}}\hat{c}^{\dagger}_{n\sigma,\mathbf{k}_{\parallel}}[\mathbf{e}_\alpha\cdot(\mathbf{m}\times\hat{\boldsymbol{\sigma}})]_{\sigma\sigma'}\hat{c}_{n\sigma',\mathbf{k}_{\parallel}}, \quad (7)$$

and $\hat{G}^r(E)[\hat{H}^q]$ is computed for the new Hamiltonian $\hat{H}^q = \hat{H}_{\mathrm{TI}} + \hat{H}^q_F$. This yields $\partial\hat{G}^r/\partial q \approx (\hat{G}^r[\hat{H}^q] - \hat{G}^r[\hat{H}])/q$, where we use $q = 10^{-7}$ as the infinitesimal. The derivative $\partial\hat{G}^r/\partial q$ plugged into Eq. (6) yields $Q = T_\alpha$.

Equation (6) includes both the equilibrium $\mathbf{T}_\perp(V_b = 0)$ [21,26,27] and experimentally measured [3] nonequilibrium $\mathbf{T}_\perp(V_b) - \mathbf{T}_\perp(V_b = 0)$ contribution to $\mathbf{T}_\perp$. The linear-response contribution can be extracted (see Sec. III in the Supplemental Material [18]) by expanding the density matrix $\hat{\rho}$ to first order in the applied bias voltage V_b and by subtracting the purely equilibrium term $\hat{\rho}_{\mathrm{eq}} = -\frac{1}{\pi}\int dE\mathrm{Im}[\hat{G}^r_0(E)]f(E)$:

$$Q_{\mathrm{neq}} = -\sum_p V_p\mathrm{Tr}\left[\frac{\partial\hat{G}^r_0}{\partial q}\hat{\Gamma}_p\hat{G}^a_0\hat{\Gamma} - i\frac{\partial\hat{G}^r_0}{\partial q}\hat{\Gamma}_p\right] - \sum_p V_p\mathrm{Im}\left\{\int_{-\infty}^{E_F} dE\mathrm{Tr}\left[\frac{\partial\hat{G}^r_0}{\partial q}\frac{\partial\hat{H}}{\partial V_p} - \frac{\partial\hat{G}^r_0}{\partial q}\frac{\partial\hat{\Sigma}^r_p}{\partial E}\right]\right\}. \quad (8)$$

Here $G^r_0(E)$ is the retarded GF at zero bias voltage and we assume zero temperature. The second sum in Eq. (8) is nonzero only for $\mathbf{T}_\perp \propto V_b$ where the integration over the

Fermi sea is necessary to ensure the gauge invariance (i.e., invariance under a global potential shift $V_p \rightarrow V_p + V_0$) of $\mathbf{T}_\perp$ plotted in Fig. 2. Note that the $\mathbf{T}_\perp \propto V_b$ component is identically zero [3,26,27] in symmetric F′/I/F MTJs, as confirmed by Fig. 2(b) using our general Eq. (8).

We conclude by noting that although the STT we predict in N/TI/F junctions does not require an F′ layer with fixed magnetization as a polarizer, its measurement necessitates usage of the second reference F′ layer in order to detect magnetization switching or precession in the free F layer. Nevertheless, the experimental setups we propose for this purpose in Sec. II of the Supplemental Material [18], consisting of a MTJ capped with a TI layer to form TI/F/I/F′ stacking, require a much smaller total number of layers than recently fabricated orthogonal STT-MRAM [16] and STT-oscillators [17] (containing an F″ polarizer whose fixed magnetization must be kept perpendicular to the in-plane magnetized F and F′ layers).

F. M. and B. K. N. were supported by DOE Grant No. DE-FG02-07ER46374. N. N. was supported by Grant-in-Aids for Scientific Research (21244053) from the Ministry of Education, Culture, Sports, Science and Technology of Japan, Strategic International Cooperative Program (Joint Research Type) from the Japan Science and Technology Agency, and also by the Funding Program for World-Leading Innovative R&D on Science and Technology (FIRST Program).

*bnikolic@udel.edu

[1] D. Ralph and M. Stiles, J. Magn. Magn. Mater. **320**, 1190 (2008); A. Brataas, A. D. Kent, and H. Ohno, Nature Mater. **11**, 372 (2012).
[2] J. A. Katine and E. E. Fullerton, J. Magn. Magn. Mater. **320**, 1217 (2008).
[3] C. Wang, Y.-T. Cui, J. A. Katine, R. A. Buhrman, and D. C. Ralph, Nature Phys. **7**, 496 (2011).
[4] I. M. Miron, G. Gaudin, S. Auffret, B. Rodmacq, A. Schuhl, S. Pizzini, J. Vogel, and P. Gambardella, Nature Mater. **9**, 230 (2010); I. M. Miron, K. Garello, G. Gaudin, P.-J. Zermatten, M. V. Costache, S. Auffret, S. Bandiera, B. Rodmacq, A. Schuhl, and P. Gambardella, Nature (London) **476**, 189 (2011).
[5] L. Liu, O. Lee, T. Gudmundsen, D. Ralph, and R. Buhrman, Phys. Rev. Lett. **109**, 096602 (2012).
[6] A. Manchon and S. Zhang, Phys. Rev. B **78**, 212405 (2008); A. Manchon and S. Zhang, *ibid.***79**, 094422 (2009); K. Obata and G. Tatara, *ibid.***77**, 214429 (2008); A. Matos-Abiague and R. L. Rodriguez-Suarez, *ibid.***80**, 094424 (2009); I. Garate and A. H. MacDonald, *ibid.***80**, 134403 (2009).
[7] P. Gambardella and I. M. Miron, Phil. Trans. R. Soc. A **369**, 3175 (2011).
[8] M. Z. Hasan and C. L. Kane, Rev. Mod. Phys. **82**, 3045 (2010).
[9] D. Pesin and A. H. MacDonald, Nature Mater. **11**, 409 (2012).
[10] I. Garate and M. Franz, Phys. Rev. Lett. **104**, 146802 (2010); T. Yokoyama, J. Zang, and N. Nagaosa, Phys. Rev. B **81**, 241410(R) (2010); T. Yokoyama, Phys. Rev. B **84**, 113407 (2011).
[11] F. Mahfouzi, J. Fabian, N. Nagaosa, and B. K. Nikolić, Phys. Rev. B **85**, 054406 (2012).
[12] A. Manchon, Phys. Rev. B **83**, 172403 (2011).
[13] F. Mahfouzi, N. Nagaosa, and B. K. Nikolić, arXiv:1112.2314.
[14] E. Zhao, C. Zhang, and M. Lababidi, Phys. Rev. B **82**, 205331 (2010); J. A. Hutasoit and T. D. Stanescu, Phys. Rev. B **84**, 085103 (2011).
[15] N. P. Butch, K. Kirshenbaum, P. Syers, A. B. Sushkov, G. S. Jenkins, H. D. Drew, and J. Paglione, Phys. Rev. B **81**, 241301 (2010); D. Kim, S. Cho, N. P. Butch, P. Syers, K. Kirshenbaum, S. Adam, J. Paglione, and M. S. Fuhrer, Nature Phys. **8**, 460 (2012).
[16] H. Liu, D. Bedau, D. Backes, J. A. Katine, J. Langer, and A. D. Kent, Appl. Phys. Lett. **97**, 242 510 (2010).
[17] D. Houssameddine *et al.*, Nature Mater. **6**, 447 (2007).
[18] See Supplemental Material at http://link.aps.org/supplemental/10.1103/PhysRevLett.109.166602 for separation of STT in Fig. 2(a) into contributions generated by the surface and bulk of the TI layer; possible experimental setups to detect such STT; and detailed derivation of the proper gauge-invariant nonequilibrium density matrix.
[19] K. M. D. Hals, A. Brataas, and Y. Tserkovnyak, Europhys. Lett. **90**, 47 002 (2010).
[20] P. M. Haney and M. D. Stiles, Phys. Rev. Lett. **105**, 126602 (2010).
[21] P. M. Haney, D. Waldron, R. Duine, A. Núñez, H. Guo, and A. MacDonald, Phys. Rev. B **76**, 024404 (2007).
[22] X. Jia, K. Xia, Y. Ke, and H. Guo, Phys. Rev. B **84**, 014401 (2011).
[23] J. C. Slonczewski, J. Magn. Magn. Mater. **159**, L1 (1996); L. Berger, Phys. Rev. B **54**, 9353 (1996).
[24] D. M. Edwards, F. Federici, J. Mathon, and A. Umerski, Phys. Rev. B **71**, 054407 (2005).
[25] S. Wang, Y. Xu, and K. Xia, Phys. Rev. B **77**, 184430 (2008).
[26] J. Xiao, G. E. W. Bauer, and A. Brataas, Phys. Rev. B **77**, 224419 (2008).
[27] I. Theodonis, N. Kioussis, . Kalitsov, M. k. Chshiev, and W. Butler, Phys. Rev. Lett. **97**, 237205 (2006); Y.-H. Tang, N. Kioussis, A. Kalitsov, W. H. Butler, and R. Car, Phys. Rev. B **81**, 054437 (2010).
[28] B. K. Nikolić and S. Souma, Phys. Rev. B **71**, 195328 (2005).
[29] I. Adagideli, G. E. W. Bauer, and B. I. Halperin, Phys. Rev. Lett. **97**, 256601 (2006).
[30] C.-X. Liu, X.-L. Qi, H. Zhang, X. Dai, Z. Fang, and S.-C. Zhang, Phys. Rev. B **82**, 045122 (2010).
[31] Z. Y. Wang, X. Guo, H. D. Li, T L. Wong, N. Wang, and M. H. Xie, Appl. Phys. Lett. **99**, 023112 (2011).
[32] M. D. Stiles and A. Zangwill, Phys. Rev. B **66**, 014407 (2002).
[33] H. Haug and A.-P. Jauho, *Quantum Kinetics in Transport and Optics of Semiconductors* (Springer-Verlag, Berlin, 2008).
[34] J.-T. Lü, M. Brandbyge, and P. Hedegård, Nano Lett. **10**, 1657 (2010); N. Bode, S. V. Kusminskiy, R. Egger, and F. von Oppen, Phys. Rev. Lett. **107**, 036804 (2011); N. Bode, L. Arrachea, G. S. Lozano, T. S. Nunner, and F. von Oppen, Phys. Rev. B **85**, 115440 (2012).

Supplemental Material for "Spin-Orbit Coupling Induced Spin-Transfer Torque and Current Polarization in Topological-Insulator/Ferromagnet Vertical Heterostructures"

Farzad Mahfouzi,[1] Naoto Nagaosa,[2,3] and Branislav K. Nikolić[1,2,*]

[1]*Department of Physics and Astronomy, University of Delaware, Newark, DE 19716-2570, USA*
[2]*Cross-Correlated Materials Research Group (CMRG) and Correlated Electron Research Group (CERG), RIKEN-ASI, Wako, Saitama 351-0198, Japan*
[3]*Department of Applied Physics, University of Tokyo, Tokyo 113-8656, Japan*

I. SEPARATION OF TOTAL TORQUE IN N/TI/F VERTICAL HETEROSTRUCTURES INTO THE SURFACE AND BULK CONTRIBUTIONS

The in-plane $\mathbf{T}_{\parallel}$ and perpendicular $\mathbf{T}_{\perp}$ torque components in conventional F′/I/F (F-ferromagnet; I-insulator) magnetic tunnel junctions (MTJs) exhibit symmetric $\propto \sin\theta$ angular dependence with respect to $\theta = 90°$ (at which the noncollinear magnetizations of reference F′ and free F layers are orthogonal to each other), as shown in Fig. 2(b) of the main text. On the other hand, when torque is driven purely by the surface spin-orbit coupling (SOC), the toque components have [1] asymmetric angular dependence around $\theta = 90°$, as demonstrated in Fig. 2(c) of the main text for N/I/F (N-normal metal) junctions with the Rashba SOC at the I/F interface (here angle θ is measured between the direction of transport and the magnetization of the free F layer).

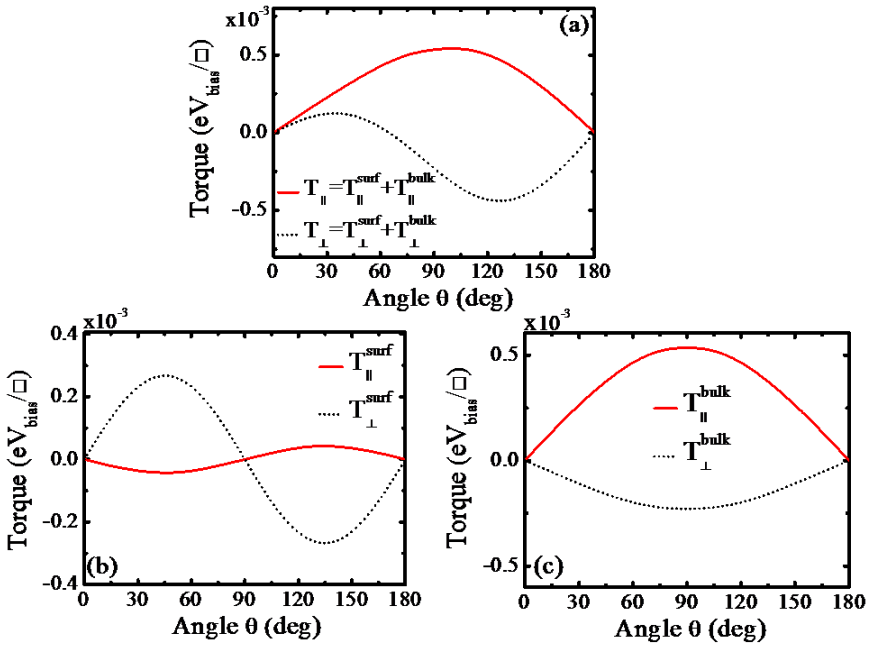

FIG. 1: (Color online) (a) The angular dependence of the in-plane $\mathbf{T}_{\parallel}$ and perpendicular $\mathbf{T}_{\perp}$ torque components, acting on the magnetization $\mathbf{m}$ of the free F layer within N/TI/F vertical heterostructure, is separated into two contributions: (b) arising from the SOC on the surface of the TI layer (i.e., at the TI/F interface); and (c) arising from the spin-polarizing effect of the bulk of the TI slab on unpolarized charge current injected perpendicularly through it (see Fig. 1 in the main text). Note that panel (a) here is identical to Fig. 2(a) in the main text.

In contrast to these two situations, the components of the torque we predict in N/TI/F (TI-topological insulator) vertical heterostructures is neither symmetric nor asymmetric around $\theta = 90°$. In the main text, we explain this feature to be the result of two different mechanisms operating concurrently: (*i*) the strong SOC on the surface of TI

*Electronic address: bnikolic@udel.edu

generates asymmetric contribution (as in N/I/F junctions); and (*ii*) spin-polarizing effect of the bulk of the TI slab on charge current flowing perpendicularly through it (see Fig. 3 in the main text) gives rise to symmetric contribution as in the case of conventional F′/I/F MTJs.

Figure 1 indeed confirms that these two contributions are simply additive, so that $\mathbf{T}_\parallel = \mathbf{T}_\parallel^{\rm surf} + \mathbf{T}_\parallel^{\rm bulk}$ and $\mathbf{T}_\perp = \mathbf{T}_\perp^{\rm surf} + \mathbf{T}_\perp^{\rm bulk}$. Furthermore, Fig. 1 shows that $\mathbf{T}_\parallel$ is dominated by the spin-polarizing effect of the bulk of the TI slab, while $\mathbf{T}_\perp$ is dominated by the torque driven by the strong surface SOC. Therefore, both $\mathbf{T}_\parallel$ and $\mathbf{T}_\perp$ have similar magnitude (except around $\theta \approx 60^\circ$ where $\mathbf{T}_\perp$ vanishes), unlike in N/I/F junctions with Rashba SOC at the I/F interface where $\mathbf{T}_\perp \gg \mathbf{T}_\parallel$ [see Fig. 2(c) in the main text].

II. PROPOSED EXPERIMENTAL SETUPS FOR DETECTION OF UNCONVENTIONAL STT IN N/TI/F VERTICAL HETEROSTRUCTURES AND POTENTIAL STT-MRAM APPLICATIONS

To detect STT in N/TI/F junction, we propose a multilayered device shown in Fig. 2 where conventional F/I/F′ MTJ is capped by a thin layer of some TI material (with another ultrathin layer of conventional band insulator in between to suppress the magnetic proximity effect on the surface of TI, as discussed in the main text). Unpolarized charge current injected across the TI slab will become polarized in the direction of transport (as shown in Fig. 3 of the main text). This effect, together with the surface contribution shown in Fig. 1 will induce switching of the free F layer, which is then detected by the second reference F′ layer in Fig. 2.

The device proposed in Fig. 2 relies on the unique properties of the unconventional STT in N/TI/F junctions, discussed in Fig. 2(a) of the main text or Fig. 1 here, and cannot be mimicked by capping the free F layer with either a heavy metal or a very thin insulator (thinner than the insulating layer I in Fig. 2) to generate sufficiently strong Rashba SOC at this interface [1, 2]. This is due to the fact that for current-perpendicular-to-plane transport in N/I/F junctions with the Rashba SOC at the I/F interface, Fig. 2(c) in the main text shows that $\mathbf{T}_\parallel$ is zero around $\theta = 0$ (i.e., when magnetization $\mathbf{m}$ in Fig. 2 is in the plane of the I/F interface), so that such torque cannot participate in the onset of magnetization switching.

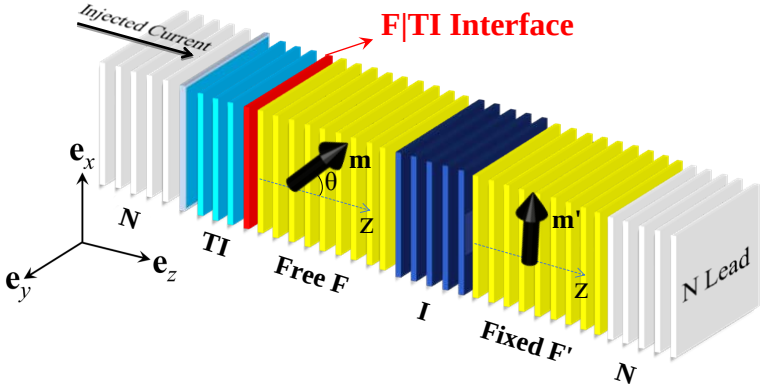

FIG. 2: (Color online) The proposed device for the detection of unconventional STT driven by perpendicular charge transport through TI slab consists of the free and reference (with fixed magnetization) ferromagnetic layers forming a conventional MTJ, where the free F layer is additionally capped by a thin layer of a TI material. Both the free and reference F layers are initially magnetized along the x-axis, while the unpolarized injected charge current flowing perpendicularly through the TI layer will become spin-polarized along the z-axis, as shown in Fig. 3 of the main text. Such spin-polarized current, together with additional torque driven by the surface SOC shown in Fig. 1(b), will switch the magnetization of the F layer which is then detected as the change in the tunneling magnetoresistance of F/I/F′ MTJ.

The device in Fig. 2 could also have substantial impact of the design of STT-operated non-volatile magnetic random access memories (MRAMs) [3] where *the key issue is switching speed*. For example, in conventional collinearly magnetized STT-MRAM devices [3], the initial current-induced STT is zero so that one has to rely on thermal fluctuations or small misalignments of the layer magnetizations to initiate the switching. This leads to undesirable long mean switching times [4] and broad switching time distributions [5]. To overcome these impediments, exploration of MTJ stacks with more than two F layers and noncollinear magnetizations has been pursued, as exemplified by the orthogonal STT-MRAM [6]. Detecting bipolar switching of the magnetization of the free F layer, which occurs for both voltage polarities, would be a clear indication that the torque is driven by the TI capping layer (rather than by thermal fluctuations of collinear magnetizations in the F/I/F′ part of the device).

The orthogonal STT-MRAM [6] contains a perpendicularly magnetized F″ layer, whose function is to spin-polarize charge current in the direction of transport, which is combined with a conventional in-plane magnetized MTJ. While this geometry has significant advantages over collinear magnetized STT-MRAM devices, as it eliminates the nanosecond incubation delays and reduces the stochastic nature of the switching, it is much more demanding to fabricate than the device proposed in Fig. 2. That is, orthogonal STT-MRAM requires more than ten different layers [6] in order to optimize spin polarization across the junction (e.g., the polarizer in the recently fabricated orthogonal STT-MRAM devices in Ref. [6] consists of a Co/Pd multilayer exchange coupled to a Co/Ni multilayer), stabilize the fixed magnetization of the reference F′ layer, and minimize stray fields.

The existence of both $\mathbf{T}_{\parallel}$ and $\mathbf{T}_{\perp}$ components of STT vector in N/TI/F junctions, akin to conventional spin valves [7] and MTJs [8, 9], makes this type of torque quite different from recently explored "SO torques" [2] that act only as an effective magnetic field which can induce switching *but not precession* of the magnetization in the free F layer. Thus, the in-plane torque component $\mathbf{T}_{\parallel}$ competes with the damping and can excite self-sustained magnetization precessions in the absence of external magnetic field (provided that in-plane and out-of plane magnetization stable states can be achieved [1]). Unlike similar scheme for N/I/F junctions [1], where one has to find a way to generate [2] sufficiently strong Rashba SOC at the I/F interface, in our N/TI/F vertical heterostructure strong SOC is guaranteed by the presence of the TI layer which also induces additional bulk contribution to $\mathbf{T}_{\parallel}$ discussed in Sec. I. Thus, the device in Fig. 2 can be used as the counterpart of STT-oscillator based on F″/F/I/F′ junction fabricated in Ref. [10] whose F″ polarizing layer, with magnetization pointing perpendicularly to initially in-plane magnetized F and F′ layers, is replaced by the TI layer.

III. THE GAUGE-INVARIANT NONEQUILIBRIUM DENSITY MATRIX FOR FINDING THE EXPECTATION VALUES OF STT VECTOR COMPONENTS

The most accurate experiments (such as those based on spin-transfer-driven ferromagnetic resonance [8]) measuring STT components $\mathbf{T}_{\parallel}$ and $\mathbf{T}_{\perp}$ have access only to their derivatives with respect to voltage (the so-called "torkance"). Thus, only the nonequilibrium contributions driven by nonzero bias voltage $V_b = V_L - V_R$ between the left and the right electrode are accessed experimentally. While $\mathbf{T}_{\parallel}$ is zero in equilibrium, $\mathbf{T}_{\perp}$ has an equilibrium contribution [11] which is nonzero at $V_b = 0$. Such equilibrium contribution should be removed when comparing theoretical predictions with experimental results.

At finite bias voltage, one can simply compute $\mathbf{T}_{\perp}(V_b) - \mathbf{T}_{\perp}(V_b = 0)$ to get the purely nonequilibrium perpendicular torque [12]. However, this straightforward approach fails at small V_b due to substantial numerical errors accumulated when subtracting two nearly equal numbers. In symmetric MTJs with identical F and F′ layers, one can eliminate the equilibrium contribution to linear-response $\mathbf{T}_{\perp}$ by using the special gauge (i.e., the reference level for the applied voltages) where voltage $-V_b/2$ is applied to the left and voltage $V_b/2$ is applied to the right reservoir [11]. This trick, however, is also not applicable to our N/TI/F vertical heterostructure which is intrinsically asymmetric.

Therefore, deriving Eq. (8) in the main text requires to construct the proper *gauge-invariant* nonequilibrium density matrix $\hat{\rho}_{\rm neq}$ for steady-state transport which then enters the trace in Eqs. (5) and (6) of the main text. In the steady-state transport regime, $\hat{\rho}$ can be expressed in terms of the lesser GF of the nonequilibrium Green function (NEGF) formalism [13]:

$$\hat{\rho} = \frac{1}{2\pi i} \int dE\, \hat{G}^{<}(E). \tag{1}$$

In the case of elastic transport regime (where electron-electron, electron-phonon, and electron-spin dephasing processes are absent), $\hat{G}^{<}(E) = \hat{G}^{r}(E)[if_L(E)\hat{\Gamma}_L(E) + if_R(E)\hat{\Gamma}_R(E)]\hat{G}^{a}(E)$ is given solely in terms of the retarded GF, $\hat{G}^{r}(E)$. Here $\hat{G}^{a}(E) = [\hat{G}^{r}(E)]^{\dagger}$ is the advanced GF, $\hat{\Gamma}_{L,R}(E) = i[\hat{\Sigma}^{r}_{L,R}(E) - \hat{\Sigma}^{a}_{L,R}(E)]$ are the level broadening operators due to the coupling to the left (L) and right (R) leads [as described by the self-energies $\hat{\Sigma}^{r}_{L,R}(E)$], and $f_{L,R}(E) = f(E - eV_{L,R})$ are the Fermi functions of macroscopic reservoirs to which the leads are assumed to be attached at infinity.

For purely computational purposes [14, 15], one usually separates "equilibrium" and "nonequilibrium" contributions to $\hat{\rho}$ in the elastic transport regime:

$$\hat{\rho} = -\frac{1}{\pi} \int\limits_{-\infty}^{+\infty} dE\, \mathrm{Im}\left[\hat{G}^{r}(E)\right] f_R(E) + \frac{1}{2\pi} \int\limits_{-\infty}^{+\infty} dE\, \hat{G}^{r}(E) \cdot \hat{\Gamma}_L(E - eV_L) \cdot \hat{G}^{a}(E)\, [f_L(E) - f_R(E)]\,. \tag{2}$$

Here the first "equilibrium" term is typically computed via the semicircular path combined with the path in the complex plane parallel to the real axis [14], while the integration of in the second "nonequilibrium" term is bounded

between $E_F - eV_R$ and $E_F - eV_L$ by the difference of the Fermi functions (E_F is the Fermi energy) and has to be done directly along the real axis [15].

While the second "nonequilibrium" term in Eq. (2) contains information about the bias voltage [through $f_L(E) - f_R(E)$], as well as about the lead assumed to be injecting electrons into the device (through $\hat{\Gamma}_L$), it cannot be used as the proper nonequilibrium density matrix which is defined by:

$$\hat{\rho}_{\rm neq} = \hat{\rho} - \hat{\rho}_{\rm eq} = \hat{\rho} + \frac{1}{\pi}\int\limits_{-\infty}^{+\infty} dE\, {\rm Im}\left[\hat{G}^r(E)\right] f(E). \tag{3}$$

That is, the second term in Eq. (3), which is the NEGF expression for the equilibrium density matrix $\hat{\rho}_{\rm eq}$, does not cancel the gauge non-invariant first term in Eq. (2) that depends explicitly [through $f_R(E)$] on arbitrarily set V_R and implicitly on the voltages applied to both reservoirs [through $\hat{G}^r(E)$].

Surprisingly enough, the second term in Eq. (2), written in the linear-response and zero-temperature limit (where it becomes the Fermi surface property)

$$\frac{1}{2\pi}\int\limits_{-\infty}^{+\infty} dE\, \hat{G}^r(E)\cdot\hat{\Gamma}_L(E-eV_L)\cdot\hat{G}^a(E)[f_L(E)-f_R(E)] \to \frac{eV_b}{2\pi}\hat{G}^r(E_F)\cdot\hat{\Gamma}_L(E_F)\cdot\hat{G}^a(E_F), \tag{4}$$

is often used in the STT literature [16, 17] as the putative "nonequilibrium" density matrix $\hat{\rho}_{\rm neq}$ which defines the expectation values through ${\rm Tr}[\ldots\hat{\rho}_{\rm neq}]$. This procedure is incorrect since, depending on the choice of voltages V_L and V_R, it will add a portion (within some energy interval) of the equilibrium perpendicular torque $\mathbf{T}_\perp(V_b = 0)$ onto the true nonequilibrium value that one is trying to compute.

To derive the proper gauge-invariant $\hat{\rho}_{\rm neq}$ in the linear-response limit, we first expand the retarded GF

$$\hat{G}^r(E) = \left[E - \hat{H} - eU - \hat{\Sigma}_L(E-eV_L) - \hat{\Sigma}_R(E-eV_R)\right]^{-1}, \tag{5}$$

to linear order in the bias voltage. Here $\hat{H}$ is the Hamiltonian of the active region of the device and eU is the potential profile across the active region of the device when current is flowing. This is achieved in two steps, where we first rewrite Eq. (5) using the exact Dyson equation [18]

$$\hat{G}^r(E) = \hat{G}^r_0(E) + \hat{G}^r_0(E)\left[eU + \hat{\Sigma}_L(E-eV_L) - \hat{\Sigma}_L(E) + \hat{\Sigma}_R(E-eV_R) - \hat{\Sigma}_R(E)\right]\hat{G}^r(E), \tag{6}$$

in terms of the retarded GF at zero bias voltage

$$\hat{G}^r_0(E) = \left[E - \hat{H} - \hat{\Sigma}_L(E) - \hat{\Sigma}_R(E)\right]^{-1}. \tag{7}$$

In the second step, we expand the self-energies

$$\hat{\Sigma}_{L,R}(E-eV_L) \approx \hat{\Sigma}_{L,R}(E) - eV_{L,R}\frac{\partial\hat{\Sigma}_{L,R}}{\partial E}\bigg|_{V_{L,R}=0}, \tag{8}$$

to linear order in voltage. Combining Eqs. (6) and (8) gives

$$\hat{G}^r(E) \approx \hat{G}^r_0(E) + \hat{G}^r_0(E)\left[eU - eV_L\frac{\partial\hat{\Sigma}_L}{\partial E}\bigg|_{V_L=0} - eV_R\frac{\partial\hat{\Sigma}_R}{\partial E}\bigg|_{V_R=0}\right]\hat{G}^r_0(E) \tag{9}$$

By plugging Eq. (9) into Eq. (3), together with the expansion of the Fermi function

$$f_{L,R}(E) \approx f(E) - eV_{L,R}\frac{\partial f}{\partial E}\bigg|_{V_{L,R}=0}, \tag{10}$$

and expansion of the level broadening operator

$$\hat{\Gamma}_L(E-eV_L) \approx \hat{\Gamma}_L(E) - eV_L\frac{\partial\hat{\Gamma}_L}{\partial E}\bigg|_{V_L=0}, \tag{11}$$

and by keeping only the terms linear in the applied voltage, we finally obtain the gauge-invariant nonequilibrium density matrix for the steady-state transport in the linear-response regime:

$$\hat{\rho}_{\rm neq} = -\frac{eV_R}{\pi}\int\limits_{-\infty}^{+\infty} dE\,{\rm Im}\left[G_0^r\right]\left(-\frac{\partial f}{\partial E}\right) - \frac{1}{\pi}\int\limits_{-\infty}^{+\infty} dE\,{\rm Im}\left[\hat{G}_0^r\left(eU - eV_L\frac{\partial\hat{\Sigma}_L}{\partial E} - eV_R\frac{\partial\hat{\Sigma}_R}{\partial E}\right)\hat{G}_0^r\right] f(E) + \frac{eV_b}{2\pi}\int\limits_{-\infty}^{+\infty} dE\,\hat{G}_0^r\hat{\Gamma}_L\hat{G}_0^a\left(-\frac{\partial f}{\partial E}\right) \tag{12}$$

In the zero-temperature limit, this expression simplifies further

$$\hat{\rho}_{\rm neq} = -\frac{eV_R}{\pi}{\rm Im}\left[G_0^r(E_F)\right] - \frac{1}{\pi}\int\limits_{-\infty}^{E_F} dE\,{\rm Im}\left[\hat{G}_0^r\left(eU - eV_L\frac{\partial\hat{\Sigma}_L}{\partial E} - eV_R\frac{\partial\hat{\Sigma}_R}{\partial E}\right)\hat{G}_0^r\right] f(E) + \frac{eV_b}{2\pi}\hat{G}_0^r(E_F)\cdot\hat{\Gamma}_L(E_F)\cdot\hat{G}_0^a(E_F), \tag{13}$$

which we employed in Eqs. (5) and (6) of the main text to obtain the final expression for the nonequilibrium torque components in Eq. (8) of the main text. We note that expansions discussed above could be performed further [18] to obtain $\hat{\rho}_{\rm neq}$ order-by-order in the applied bias voltage.

The gauge-invariant expression Eq. (13) for $\hat{\rho}_{\rm neq}$ is quite different from often [16, 17] used but incorrect Eq. (4). It is also much more computationally demanding since not all quantities in it are the Fermi surface property—the second term in Eq. (13) requires integration from the bottom of the band up to the Fermi energy. When computing the nonequilibrium $\mathbf{T}_\perp$ using Eq. (6) in the main text via trace of the product of $\partial\hat{G}^r/\partial q$ and $\hat{\rho}_{\rm neq}$, we use the fact that integrand in the second term in Eq. (13) is analytic function in the upper complex plane. Then such integration can proceed along the infinite semi-circle, where the trace is zero due to $\partial\hat{G}^r/\partial q \sim 1/E^2$, plus the vertical line at $E = E_F$ (where adaptive integration is required very lose to E_F).

For junctions with transverse translational symmetry, such as the one in Fig. 1 of the main text, one has to perform additional integration over $\mathbf{k}_\parallel$. This requires adaptive scheme (or very dense k-point sampling in brute force schemes [7]) to converge the integrand because of the fact that STT can change fast in the some regions of the 2D Brillouin zone (such as in its center in the case of N/TI/F junctions or throughout in the case of N/I/F junctions with the Rashba SOC at the I/F interface).

We conclude by noting that while the key experimental issues for STT in conventional MTJs is its control via finite bias voltage [8], and Eq. (6) in the main text intrinsically takes into account finite bias voltage, the effective Hamiltonian Eq. (3) in the main text is too crude to describe the band structure of a real 3D TI material necessary for such calculations. Similarly, the computation of nonequilibrium $\mathbf{T}_\perp \propto V_b$ for N/TI/F junction requires integration over the whole energy band so that our result for $\mathbf{T}_\perp$ in Fig. 1 is also crude. Reliable integration over energy or finite bias calculations necessitate coupling of Eq. (6) in the main text to NEGF-DFT formalism [19] to capture the band structure and interface reconstruction, as well as the self-consistent charge and spin densities across the junction.

[1] A. Manchon, Phys. Rev. B **83**, 172403 (2011).
[2] P. Gambardella and I. M. Miron, Philos. Transact. A Math. Phys. Eng. Sci. **369**, 3175 (2011).
[3] J. Katine and E. E. Fullerton, J. Magn. Magn. Mater. **320**, 1217 (2008).
[4] T. Devolder *et al.*, Phys. Rev. Lett. **100**, 057206 (2008).
[5] D. Bedau *et al.*, Appl. Phys. Lett. **97**, 262502 (2010).
[6] H. Liu *et al.*, Appl. Phys. Lett. **97**, 242510 (2010).
[7] S. Wang, Y. Xu, and K. Xia, Phys. Rev. B **77**, 184430 (2008).
[8] C. Wang *et al.*, Nature Phys. **7**, 496 (2011).
[9] S.-C. Oh *et al.*, Nature Phys. **5**, 898 (2009).
[10] D. Houssameddine *et al.*, Nature Mater. **6**, 447 (2007).
[11] J. Xiao, G. E. W. Bauer, and A. Brataas, Phys. Rev. B **77**, 224419 (2008).
[12] Y.-H. Tang *et al.*, Phys. Rev. B **81**, 054437 (2010).
[13] H. Haug and A.-P. Jauho, *Quantum kinetics in transport and optics of semiconductors* (Springer, Berlin, 2007).
[14] M. Brandbyge *et al.*, Phys. Rev. B **65**, 165401 (2002).
[15] D. A. Areshkin and B. K. Nikolić, Phys. Rev. B **81**, 155450 (2010).
[16] P. M. Haney *et al.*, Phys. Rev. B **76**, 024404 (2007).
[17] C. Heiliger *et al.*, J. Appl. Phys. **103**, 07A709 (2008).
[18] A. R. Hernández and C. H. Lewenkopf, arXiv:0907.2073.
[19] X. Jia, K. Xia, Y. Ke, and H. Guo, Phys. Rev. B **84**, 014401 (2011).